

Article

Sensitive Detection of Silicon in Aqua Phase by Microwave-Assisted Laser-Induced Breakdown Spectroscopy

Ali M. Alamri  and Zeyad T. Alwahabi * 

School of Chemical Engineering, University of Adelaide, Adelaide, SA 5005, Australia; ali.alamri@adelaide.edu.au

* Correspondence: zeyad.alwahabi@adelaide.edu.au

Abstract: Microwave-assisted laser-induced breakdown spectroscopy (MA-LIBS) was demonstrated to be an effective method for the quantitative detection of silicon in the aqua phase. Microwave radiation was transmitted into plasma using a near-field applicator device under ambient pressure and temperature conditions. Silicon detection was performed directly on the surface of a water jet. Two Si emission lines, 251.6 nm and 288.16 nm, were selected to evaluate the MA-LIBS enhancement and determine the limit of detection for silicon. The signal-to-noise ratio of the MA-LIBS spectra was investigated as a function of laser energy and microwave power. The calibration curve was established for Si quantitative analysis using 8 mJ of laser energy and 900 W of microwave power. The MA-LIBS recorded a 51-fold and 77-fold enhancement for Si I 251.6 nm and 288.16 nm, respectively. Reducing liquid splashes after laser ablation is essential to improving the quantitative analysis. Using MA-LIBS reduced the liquid splashes due to MA-LIBS using 8 mJ. The detection limit achieved was 1.25, a 16-fold improvement over traditional LIBS.

Keywords: laser-induced breakdown spectroscopy; LIBS; microwave-assisted laser-induced breakdown spectroscopy; MA-LIBS; signal enhancement; liquid plasma; detection limit



Citation: Alamri, A.M.; Alwahabi, Z.T. Sensitive Detection of Silicon in Aqua Phase by Microwave-Assisted Laser-Induced Breakdown Spectroscopy. *Photonics* **2024**, *11*, 380. <https://doi.org/10.3390/photronics11040380>

Received: 26 March 2024

Revised: 10 April 2024

Accepted: 13 April 2024

Published: 17 April 2024



Copyright: © 2024 by the authors. Licensee MDPI, Basel, Switzerland. This article is an open access article distributed under the terms and conditions of the Creative Commons Attribution (CC BY) license (<https://creativecommons.org/licenses/by/4.0/>).

1. Introduction

Laser-induced breakdown spectroscopy (LIBS) is a spectrochemical analytical technique that provides qualitative and quantitative information about an analyte using an emission emitted from a plasma created by a short laser pulse [1]. Compared to a conventional analytical technique, such as inductively coupled plasma mass spectroscopy (ICP-MS), LIBS requires minimal to no sample pretreatment, while the sample requires dilution before the ICP-MS measurement. MS spectrometers work under vacuum conditions, while LIBS works in open air under ambient pressure [2]. LIBS is a mobile and in situ analysis technique, while ICP-MS is the opposite [3]. The time measurement in LIBS is instant, while it is seconds in ICP-MS. LIBS suffers from low sensitivity, which causes a high detection limit (LoD), where the LIBS LoD is a few hundred ppm [4], while that of ICP-MS is a few ppb [5]. Therefore, approaches have been invented to cope with LIBS's drawbacks, including double-pulse LIBS (DP-LIBS), LIBS assisted by laser-induced fluorescence and microwave-assisted LIBS (MA-LIBS) [6–10].

Silicon, in the form of silica dissolved in water, is used in desalination and power plants to purify water by removing suspended particles. The addition of sodium oxide to low concentrations of dissolved silica in water results in the formation of sodium silicate, which inhibits corrosion inside steam turbines and water systems [11,12]. However, a high silica concentration has a negative impact because it forms a glassy layer on the internal surfaces of turbine boilers, pipes and blades, which causes thermal and steam-flow deficiencies when temperatures and pressures are high inside the system [13,14]. In addition, at high concentrations and ambient temperatures, sodium silicate ceases to inhibit corrosion and instead creates corrosion [12,15]. Therefore, techniques employed to monitor silica concentrations include atomic absorption spectroscopy [16], colourimetric

methods (yellow and blue silicomolybdic acid procedures) [17], inductively coupled plasma optical emission spectroscopy, inductively coupled plasma mass spectroscopy [18], flow injection [19,20] and laser-induced breakdown spectroscopy (LIBS) [21].

Sabsabi and Cielo calibrated the Si 251.6 nm emission line in an aluminium alloy using LIBS. The calculated limit of detection (LoD) was 14 ppm [22]. Zheng et al. demonstrated LIBS for the defence waste vitrification process. The established calibration curve was obtained by recording Si 288 nm emission line intensities at different Si concentrations in the CeO₂ matrix after ablation, and the calculated LoD was 40 ppm [23]. De Souza et al. calculated the LoD of Si in a matrix of sugar cane leaves using LIBS. The study objectified two Si emission lines: 212.4 nm and 288.16 nm. The resulting LoDs were 160 and 20 ppm using the Si 212.4 nm and 288.16 nm emission lines, respectively. The difference in LoDs due to the Si 288.16 nm emission line was more intense than that due to the 212.4 nm emission line [24]. Skrzeczanowski et al. improved LIBS's analytical performance by applying a liquid-to-solid conversion process to a Si solution, particularly the substrate absorption method. The calculated LoD was 5.2 ppm [25]. Yaroshchuk et al. used the substrate absorption method as a sample pretreatment. In addition, they used a secondary source of energy to prolong the LIBS plasma's life in a so-called double-pulse LIBS (DP-LIBS). The calculated LoDs were 19 and 11 in engine oil using LIBS and DP-LIBS [26].

Steel alloy is a popular host matrix for Si LIBS analysis. For example, Zhang et al. used steel alloy to perform Si analysis using two techniques: LIBS and LIBS assisted with laser-induced molecular fluorescence (LIBS-LIMF). In the LIBS analysis, the Si 288.16 nm emission line intensities were recorded at different concentrations of Si in a steel alloy to establish the calibration curve. In LIBS-LIMF, however, the SiO molecular emission line intensities were the target. The LoDs were 2014 ppm and 187 ppm for LIBS and LIBS-LIMF, respectively [27]. Moreover, Abdulmadjid et al. conducted an experiment to calculate the LoD of Si in steel alloy using picosecond LIBS at low He pressure. The calculated LoD was 15 ppm [28]. Aragon et al. calculated 80 ppm Si LoD in a steel alloy matrix using LIBS under the atmospheric pressure of Ar [29]. Ismail et al. analysed Si quantitatively in steel alloy using LIBS and DP-LIBS. The calculated LoDs were 100 ppm using LIBS and 40 ppm using DP-LIBS [30].

MA-LIBS offers remarkable enhancements to LIBS sensitivity, consuming low levels of laser energy. Kasim et al. recorded an MA-LIBS signal for 50 ppm Ru, while the LIBS signal for the same element was not recordable even at concentrations of 600 ppm; the MA-LIBS LoD was 957 ppb, and the signal-to-noise ratio was improved 76-fold for Ru using 10 mJ laser energy and 750 W microwave power [31]. Ikeda et al. recorded 49-fold, 966-fold and 1292-fold signal enhancements for Cr I, Al I and Pb I lines using 2 mJ of laser energy and 1 kW of microwave power in different sample matrices [32]. Viljanen et al. recorded a 100-fold signal enhancement and a 93-fold LoD improvement for Cu I using 2.6 mJ of laser energy and 1.2 kW of microwave power [33]. Wakil et al. recorded silver emissions in solid and liquid samples using MA-LIBS; while LIBS did not detect a signal, the LoDs for MA-LIBS were 4.5 ppm and 0.4 ppm silver in the solid and liquid samples, respectively. Wall et al. found that the MA-LIBS signal and LoD were 60-fold and 11.5-fold better than LIBS, respectively, when 6.7 mJ of laser energy and 1.2 kW of microwave power were used [34].

MW-LIBS also successfully detects molecular emissions. Wakil et al. detected CaCl, CaF and CaBr emissions lines to calibrate Cl I, F I and Br I lines in two separate studies; the LoD improvements were threefold for Cl I and fourfold for the F I and Br I lines [35,36]. Ikeda et al. observed OH and N₂ emissions using MA-LIBS in air plasma under ambient pressure, but they were not observed when LIBS was used [37,38]. In addition to these MA-LIBS benefits, MA-LIBS is capable of successfully recovering LIBS signals from self-absorption [39,40].

If the analysis is customised in the liquid phase, LIBS suffers from difficulties in performing the analysis in the liquid phase due to the employment of a high level of laser energy and the short life of the liquid plasma. The high laser energy creates a strong shock

wave, which causes the liquid to splash and the surface to ripple. Consequently, the optical system is contaminated, and plasma is formed out of phase, leading to decreased LIBS sensitivity [6,41]. The short life of the plasma is caused by the quenching effect, where the plasma temperature in the liquid phase drops faster than in the solid phase, which also affects LIBS sensitivity [42]. However, MA-LIBS is a technique that provides simultaneous features, low laser energy consumption and long plasma life, which eliminate the splashes and the quenching effect, as was mentioned in the MA-LIBS literature.

To the best of the authors' knowledge, the current study reports direct silicon analysis in the liquid phase for the first time. Long-scan MW-LIBS spectra were recorded with and without microwaves to identify a suitable line for Si detection. The signal-to-noise ratio (SNR) of the MA-LIBS spectra was measured at different microwave powers and laser energies to identify optimum laser energy and microwave power. Finally, LoDs were calculated for Si 251.6 nm and 288.16 nm emission lines with and without microwave assistance.

2. Materials and Methods

Figure 1 shows the experimental setup. A 10-Hz Q-switched Nd:YAG laser (Brilliant B, Quantel) with a 532 nm wavelength and ~8 ns pulse width was used. A Glan-Laser polariser and a half-wave plate were used to control the energy of the laser pulses. The laser energy was measured using a digital power meter (Thorlab PM 100D) before the beam was focused onto the jet surface of the sample using a UV-fused lens (100 mm focal length, L1). A bifurcated fibre bundle, Y-cables, (Thorlabs BFY400HS02) was used to collect the plasma emission. The common end of the fibre was connected to an x-y translator, and one of the other two ends was connected to the spectrometer (Andor Shamrock 500i). The common end of the fibre, located 20 mm from the sample, harvested the plasma emission. It was observed that locating the fibre at 20 mm away from the plasma was sufficient to capture strong plasma emission without any optical collecting system. The laser energy was kept below 10 mJ per pulse to minimise the water splash, reducing the risk of blocking the fibre optical end. The spectrometer was equipped with three gratings, namely, 1200, 2400 and 3600 lines/mm diffraction gratings. The resolving power calculation is expressed as $\lambda/\Delta\lambda$ [43,44]. Here, λ is the wavelength at the maximum height of the intensity line, and $\Delta\lambda$ is the wavelength difference between λ and the wavelength of the nearest emission line. The resolving power, at 360 nm, was 5000, 10,000 and 16,000 for the 1200, 2400 and 3600 lines/mm diffraction gratings, respectively. An intensified charge-coupled device camera (Andor iStar) was attached to the spectrometer to record the spectral lines.

A microwave generator (3 kW water-cooled Sairem) provided a microwave pulse at 2.45 GHz. The microwave radiation passed through a WR340 waveguide to a three-stub impedance tuner and then through a quartz window to the waveguide-to-coaxial adapter (WR340RN). The adapter was connected to a coaxial cable (a 50 ohm NN cable 1 m long with a 0.14 dB insertion loss at 2.45 GHz). The end of the cable was connected to a near-field applicator (NFA), which delivered the microwave radiation into the plasma [45].

The tip of the NFA was positioned approximately 0.5 mm horizontally and 1.5 mm vertically with respect to the surface of the water jet and created a 40° incline. The reflection of microwave power was measured by a crystal detector consisting of a generator coupled to an isolator. The microwave pulse, 1.3 ms, started 337 µs before the laser was fired. The microwave power and pulse duration were controlled by a pulse generator (Aim-TTi) [46].

To generate a continuous water jet, the three-roller pump head of a peristaltic pump (Ismatec, MW-MS 1) was attached at one end to a 50 mL reservoir and at the other to a 0.8 mm diameter nozzle. The flow rate of the water jet was set to 0.26 mL/min. A funnel collected the water and delivered it to a plastic pipe to return it to the reservoir. The experiment was performed at room temperature under ambient pressure conditions.

The Si solution sample contained 10,000 ppm silicon dissolved in 500 mL of H₂O and was purchased from Choice Analytical Pty Ltd. A Si calibration curve from 40 ppm to 2000 ppm in deionised water was created using a 1.000 ± 0.005 mL volumetric pipette and a 50.0 ± 0.5 mL graduated cylinder.

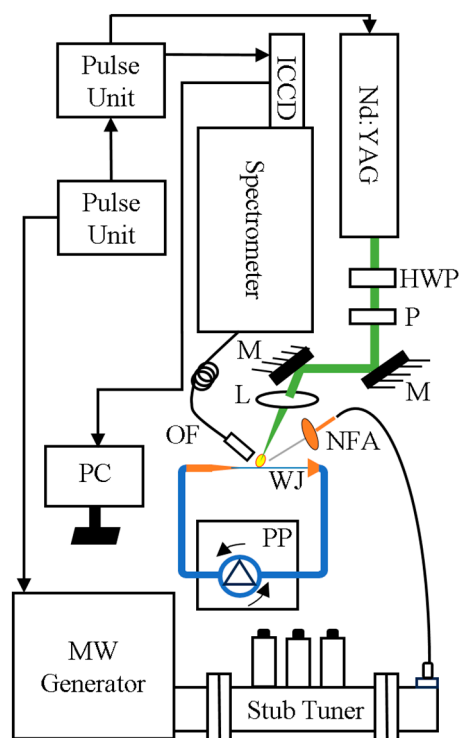


Figure 1. Schematic of microwave-assisted LIBS. L, lens; WJ, water jet; PP, peristaltic pump; NFA, near-field applicator; OF, optical fibre; HWP, half-wave plate; M, mirror; and P, polariser.

3. Results and Discussion

The ultraviolet radiation wavelength region contains a density of Si emission lines, which are featured by the highest probability of electronic transitions ($\geq 10^8 \text{ S}^{-1}$) [47]. Therefore, LIBS and MA-LIBS targeted the wavelength range from 200 to 300 nm. The targeted wavelength range contains NO $A^2\Sigma^+ \rightarrow X^2\Pi$ electronic transition from 200 nm to 250 nm [48]. The NO molecular emissions significantly affect the Si emission lines, as discussed in the following paragraph. Therefore, the present study focused on spectral lines with a transition probability equal to or higher than 10^7 S^{-1} . Figure 2 shows the LIBS and MW-LIBS spectra over the targeted spectral range.

Table 1 lists the spectral information of the Si lines located in the targeted wavelength range. The Si lines were numbered to facilitate discussion of the results. Si emission lines 1 and 8 were unresolved due to their overlap with the NO $A^2\Sigma^+ \rightarrow X^2\Pi$ (2-0 and 0-0) vibrational band wavelengths, as shown in Figure 2a,c. Also, lines 9 and 17 were unresolved due to overlapping with emissions unknown to the authors, as shown in Figure 2e,g. On the other hand, the lines were undetectable by LIBS, as shown Figure 2b,d,h, except line 9, which was detectable, as shown in Figure 2f. The narrow interspaces among the emission lines 3–7 and 11–15, and the next signals causing partial and complete spectral interference, are shown in Figure 2c,e,g. In addition, emission lines 3–7 were located within the NO $A^2\Sigma^+ \rightarrow X^2\Pi$ (0-0 and 0-1) vibrational band emission wavelength range, which caused other spectral interference to the same lines. Spectral interference increased the background emission, which reduced the enhancement of MA-LIBS and affected the reliability of the LoD [49,50]. Therefore, Si lines 3–7 and 11–15 were excluded from the Si quantitative analysis. One exception to this was Si line 12, detected using MA-LIBS, which was appropriate for the analysis because its interference with 11 and 13 was reduced by a 3600 lines/mm diffraction grating, as shown in Figures 4b and 6b. However, the Si emission lines detected using LIBS were less affected by spectral interference because NO molecular emissions were undetectable by LIBS, as shown in Figure 2d,f,h. Line 16 was undetectable by both techniques, as shown in Figure 2g,h. Previously, the appropriate emission lines for Si quantitative analysis were 2, 10, 12 and 18 due to the free spectral interference of

those lines. Si line 2 was included in the appropriate lines for the analysis, although the line overlapped with the NO $A^2\Sigma^+ \rightarrow X^2\Pi (1-0)$ emissions on the left side of the line because the NO emissions did not contribute to the maximum intensity of the Si line. The MA-LIBS enhancement for Si emission lines 2, 10 and 18 was 30-fold, 45.5-fold and 57.6-fold. The enhancement was calculated by dividing the MA-LIBS intensity by the LIBS intensity for each emission line. The intensity was calculated by subtracting the maximum height of the intensity from the background level. The background level was determined by calculating the mean of the lowest fluctuation level of the noise intensities between 255 nm and 256 nm wavelengths [51].

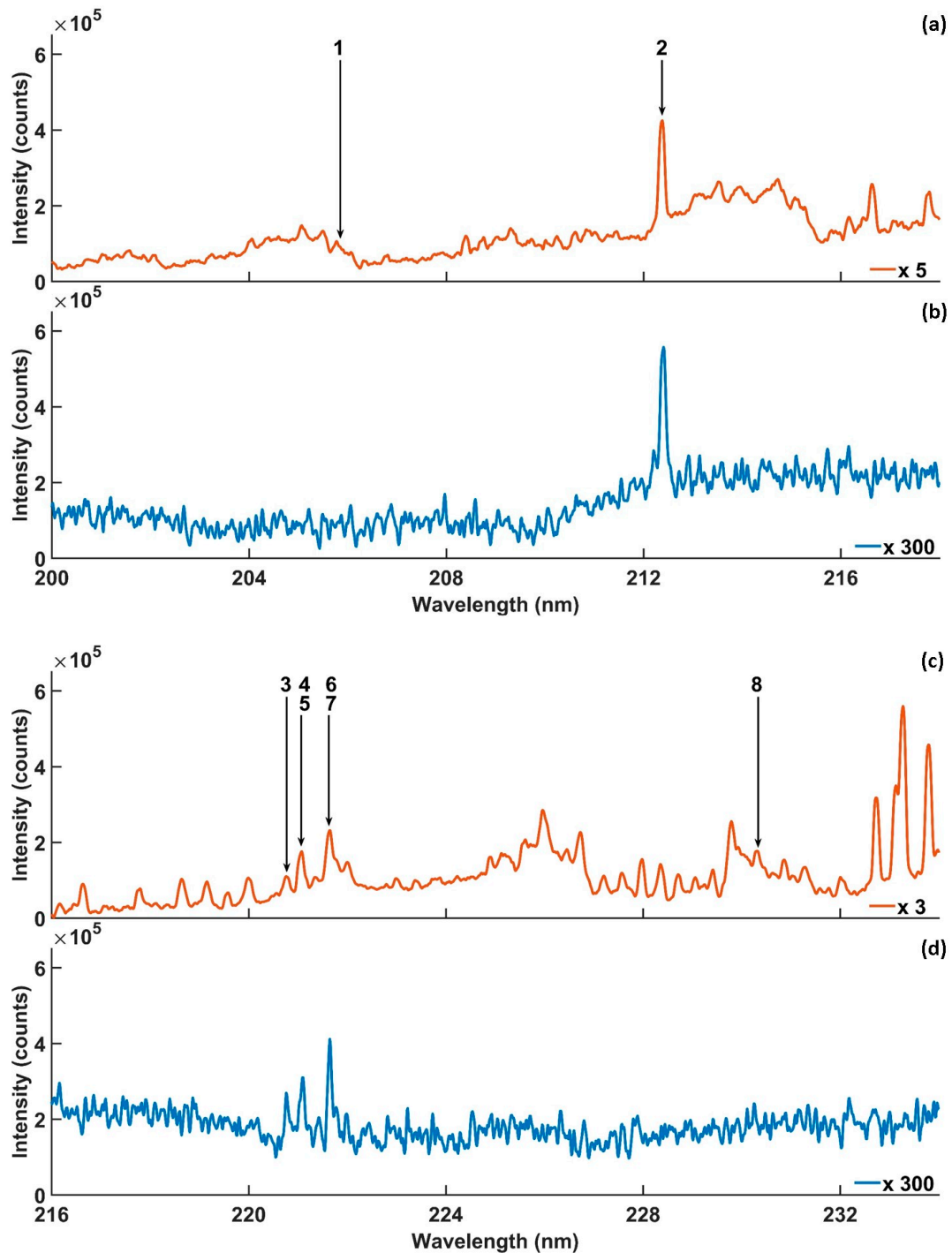


Figure 2. Cont.

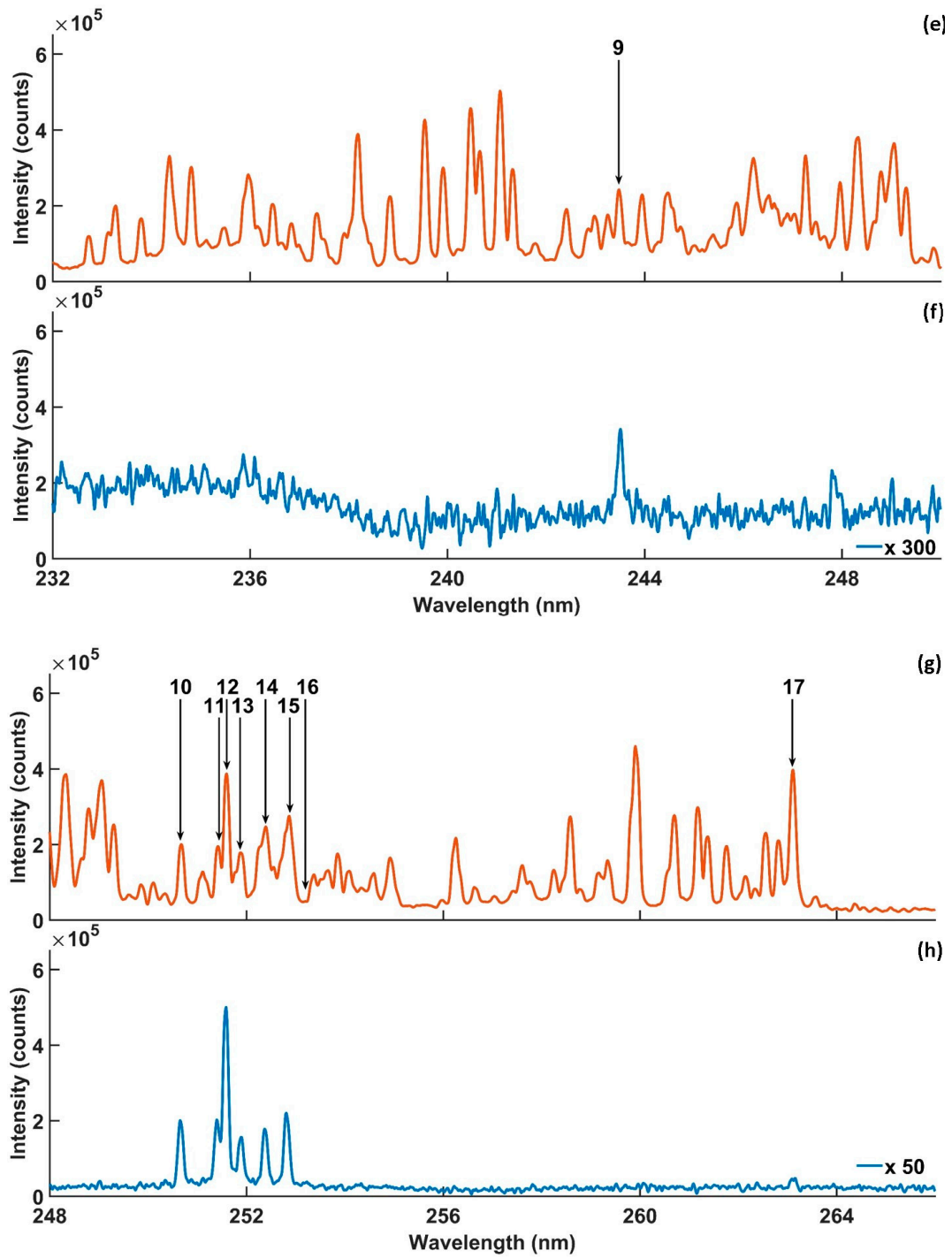


Figure 2. Cont.

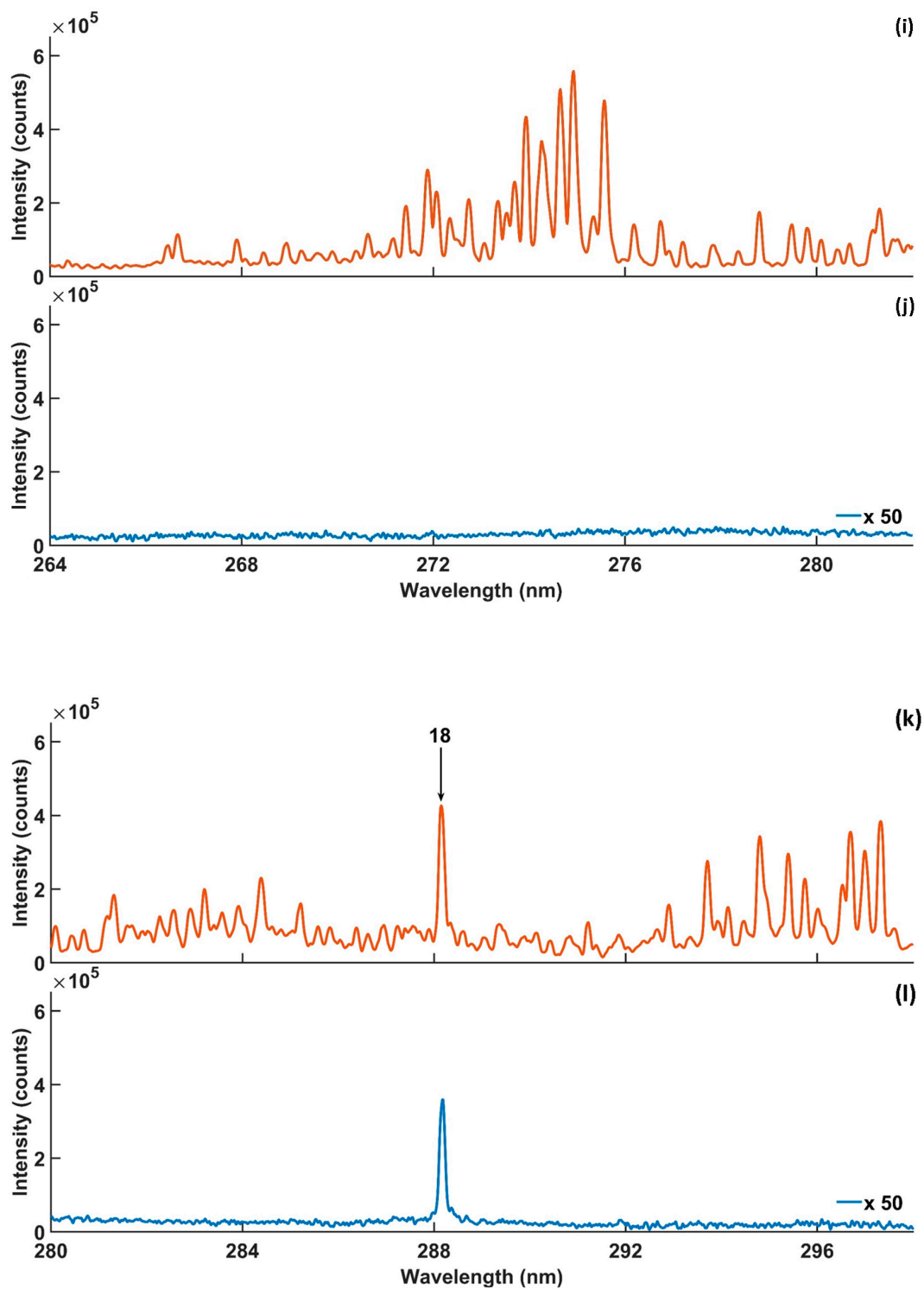


Figure 2. Microwave-assisted LIBS spectra, (a–l), obtained using 0.4% concentration of Si in silicon solution with microwave on (orange) and with microwave off (blue). Experimental parameters: laser energy = 8 mJ; microwave power = 900 W; gate width = 900 μ s; diffraction grating = 2400 lines/mm; accumulated signals = 100; gate delay = 400 ns.

High-intensity strength is required for quantitative analysis due to the reduction in the LoD and the self-absorption effect [52,53]. As a result, the Si 288.14 nm emission is the most favourable emission line for Si quantitative analysis using MA-LIBS and LIBS, as shown in Figure 2k,l. The Si 251.6 nm emission line was also appropriate for the analysis due to its

intensity, which was no less than the 288.14 nm emission line intensity for both techniques, as shown in Figure 2g,h. In addition, the recorded LoDs using the 251.6 nm emission line in the literature were competitive with the LoDs using the 288.14 nm emission line (Table 2). Therefore, the present study employed the Si 251.6 nm and 288.14 nm emission lines for the Si quantitative analysis.

Table 1. Spectral information and MA-LIBS enhancement of Si emission lines.

No.	λ (nm)	A_{ki}	E_k (eV)	E_i (eV)	Enhancement Factors
1	205.81	7×10^7	6.8	0.08	Unresolved
2	212.41	3×10^8	6.6	0.78	30
3	220.8	2.6×10^7	5.61	0.00	Spectral interference
4	221.1	3.5×10^7	5.61	0.009	Spectral interference
5	221.17	1.8×10^7	5.61	0.009	Spectral interference
6	221.67	4.5×10^7	5.62	0.027	Spectral interference
7	221.8	1.1×10^7	5.61	0.027	Spectral interference
8	230.3	3.5×10^8	7.3	1.90	Unresolved
9	243.5	4.4×10^7	5.87	0.78	Unresolved
10	250.7	5.5×10^7	4.95	0.009	45.5
11	251.43	7.4×10^7	4.93	0.00	Spectral interference
12	251.61	1.7×10^8	4.95	0.027	Spectral interference
13	251.92	5.5×10^7	4.93	0.009	Spectral interference
14	252.41	2.2×10^8	4.92	0.009	Spectral interference
15	252.85	9×10^7	4.93	0.027	Spectral interference
16	253.24	2.5×10^7	6.8	1.90	Undetectable
17	263.13	1.1×10^8	6.62	1.90	Unresolved
18	288.16	2.2×10^7	5.08	0.78	57.6

MA-LIBS was approved for molecular detection due to its high sensitivity [35,36,54]. In the present study, MA-LIBS detected OH $A^2\Sigma^+ \rightarrow X^2\Pi$ (1-0) transition emission in addition to NO molecular emission, as shown in Figure 2k. The OH (1-0) vibrational band head was located at 281.2 nm and extended to 298 nm. However, the molecular spectra were undetectable using LIBS, as shown in Figure 2l. Si emission line 18 was within the OH vibrational band wavelength range. The emission line was not affected by OH emission due to the weak OH band emissions and the strong intensity of Si emission line 18. It is noteworthy that the NO and OH emission lines were emitted from the ionisation of air molecules surrounding the microwave plasma’s periphery.

Due to the MA-LIBS LoD being directly related to the reciprocal of SNR, a high SNR is beneficial for improving MA-LIBS LoD. Therefore, optimising laser energy and microwave power allows for the achievement of the highest possible SNR value. Figure 3 shows the linear relationship between the SNRs of the MA-LIBS spectra and the microwave powers for the two different values of laser energy, 8 mJ and 10 mJ. There was a negligible difference between the SNRs of the MA-LIBS spectra at 8 mJ and 10 mJ. The values of SNR were constant while the laser energy increased, indicating the high electron density that was excited by both energies. At an electron density below the critical, the microwave re-activates the de-excited electrons; the reactivation process is explained in the following paragraphs. As the microwave power increased, the number of re-activated electrons increased, which led to an increase in the Si intensity and noise. Because the increased rate of intensity with microwave power increase was higher than the increased rate of noise, the

SNR increased with the increase in microwave power [45]. The preferable laser energy level was 8 mJ due to reduced splash, which protected the optical system from contamination. In addition, values for a power greater than 900 W were excluded from the current study due to their strong splashes. Therefore, 8 mJ and 900 W were the optimum laser energy and microwave power, respectively. The SNRs were calculated by dividing the intensity by the standard deviation of the noise intensity range. The calculation of the intensity and noise intensity range is explained in the above discussion. The minimum laser energy needed to generate a plasma was roughly 4 mJ.

Table 2. Summary of direct silicon LoD.

Technique	Detection Phase	Laser Energy (mJ)	Matrix	λ (nm)	LoD (ppm)	Ref.
LIBS	Solid	60	Al alloy	251.6	14	[22]
LIBS	Solid	25	CeO ₂	288.16	40	[23]
LIBS	Solid	25	CeO ₂	288.16	60	[23]
LIBS	Solid	220	Leaves	212.4	160	[24]
LIBS	Solid	220	Leaves	288.16	20	[24]
LIBS	Solid	50	Paper	288.16	5.2	[25]
LIBS	Solid	70	Paper	251.6	19	[26]
DP-LIBS	Solid	70	Paper	251.6	11	[26]
LIBS	Solid	60	Steel alloy	288.16	2014	[27]
LIBS-LIMFG ^a	Solid	60	Steel alloy	248.68	335	[27]
LIBS-LIMFE ^b	Solid	60	Steel alloy	248.68	187	[27]
LIBS, in He, 2.6 kPa	Solid	15	Steel alloy	251.6	15	[28]
LIBS, in Ar, ambient pressure	Solid	100	Steel alloy	288.16	80	[29]
LIBS	Solid	50	Steel alloy	288.16	100	[30]
DP-LIBS	Solid	50	Steel alloy	288.16	40	[30]
LIBS	Liquid	8	Water	251.6	53	This study
LIBS	Liquid	8	Water	288.16	18.3	This study
MA-LIBS	Liquid	8	Water	251.6	3.3	This study
MW-LIBS	Liquid	8	Water	288.16	1.25	This study

^a Laser-induced molecular fluorescence, ground state; ^b laser-induced molecular fluorescence.

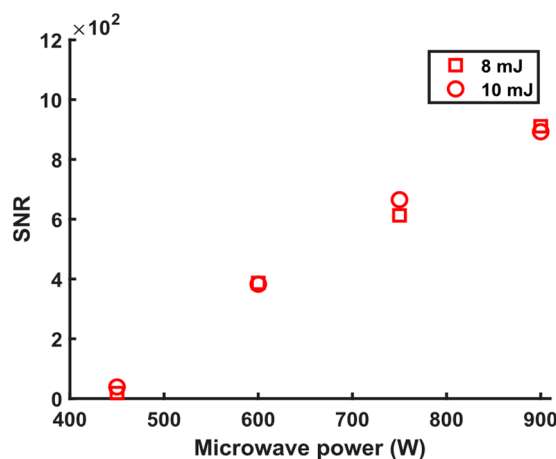


Figure 3. Signal-to-noise ratio (SNR) of MA-LIBS spectra was obtained from a silicon solution sample at different microwave powers and laser energies. Experimental parameters: gate width = 900 μ s; accumulated spectra = 100; diffraction grating = 3600 lines/mm; gate delay = 400 ns.

Figure 4 shows the MA-LIBS enhancement for the Si 251.6 nm and 288.16 nm emission lines using 3600 lines/mm diffraction grating. The Si emission lines were recorded at 2000 ppm and 400 ns using 8 mJ of laser energy and 900 W of microwave power. Numerically, the MA-LIBS Si I 251.6 nm and 288.16 nm emission intensities were 51-fold and 77-fold greater than their counterparts that used LIBS at a 2000 ppm concentration.

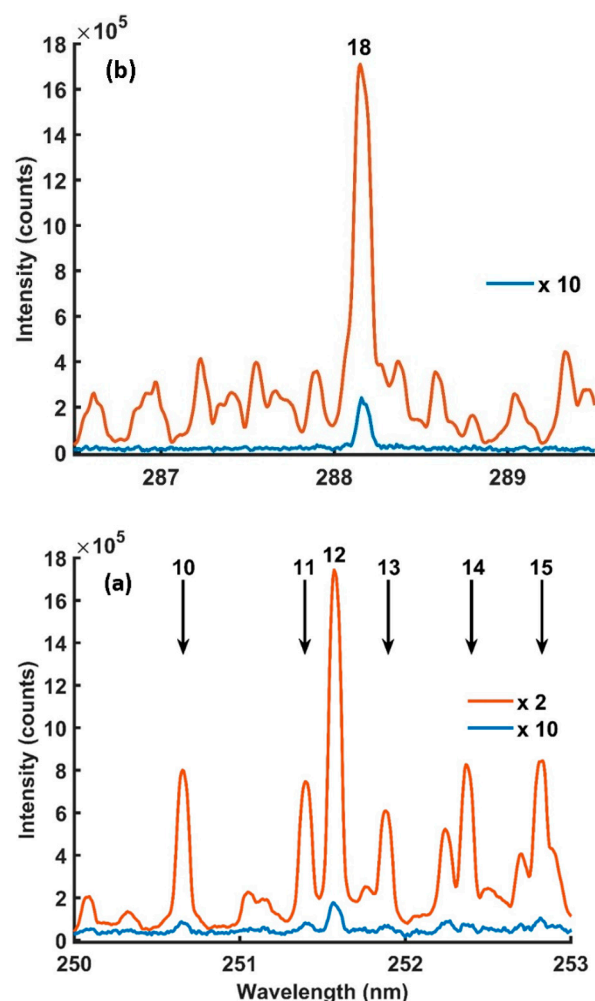


Figure 4. Microwave-assisted LIBS spectra were obtained from silicon solution: (a) Si 251.6 nm and (b) 288.16 nm emission lines with microwave on (orange) and with microwave off (blue). Experimental parameters: laser energy = 8 mJ; microwave power = 900 W; gate width = 900 μ s; diffraction grating = 3600 lines/mm; accumulated signals = 100; gate delay = 400 ns.

MA-LIBS enhancement refers to the ability of microwave radiation to extend the life of the plasma to 900 μ s in so-called microwave–plasma coupling. The mechanism of microwave coupling is as follows. After ablation, the plasma’s high electron density (to the order of 10^{19} cm^{-3}) starts to decrease. At an electron density below the critical level (7×10^{10} cm^{-3} for radiation at 2.45 GHz), the free electrons in the plasma are influenced by microwave radiation [55], where the latter provides kinetic energy to the free electrons. The energetic electrons undergo collisions with de-excited neutral atoms, which causes the atoms to jump to an excited state. Then, the re-excited atoms return to the ground state energy level by spontaneously releasing emitting energy as an emission. The released emissions carry both qualitative and quantitative information about the atom. The coupling process continues until the end of the microwave radiation pulse.

Another reason for MA-LIBS enhancement is the enlargement of the plasma, which allows the optical fibre to gain more emission during the coupling process. The enlargement process due to the microwave radiation reactivates the de-excited species in the outer shell of the plasma [56,57].

In agreement with NIST, Si 251.6 nm intensity is half that of Si 288.16 nm using a 3600 lines/mm diffraction grating under ambient pressure in open air. Therefore, Si 288.16 nm is better for establishing a calibration curve to achieve the lowest LoD for Si. This was proven by the data discussed in the next section.

Figure 5a,b and Figure 6a,b show the detected Si 251.6 nm and 288.16 nm emission lines with and without microwaves at different silicon concentrations. The intensities were detected using 8 mJ of laser energy, 900 W of microwave power, a 900 μs gate width and 400 ns of gate delay.

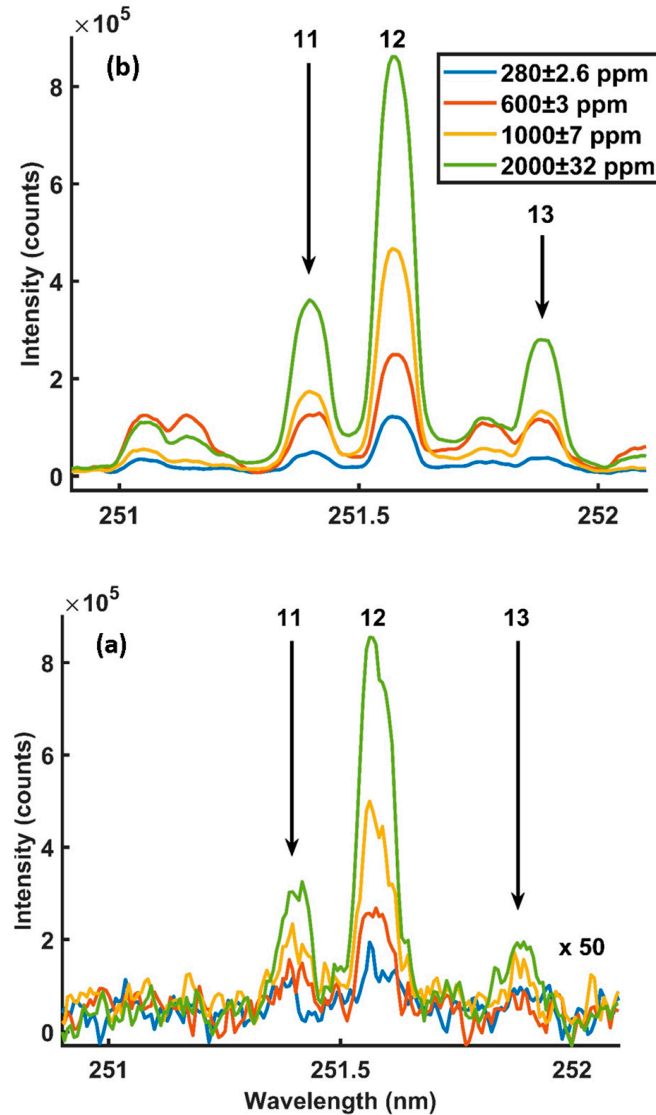


Figure 5. MA-LIBS spectra were obtained at different silicon concentrations using a Si 251.6 nm emission line: (a) microwave off and (b) microwave on. Experimental parameters: laser energy = 8 mJ; microwave power = 900 W; gate width = 900 μs; diffraction grating = 3600 lines/mm; accumulated signals = 100; gate delay = 400 ns.

The corrected Si intensities for LIBS and MW-LIBS were plotted against their concentrations, as shown in Figure 7. A linear fitting was used to establish the best slope of the line. The LoDs were calculated using the 3 σ method ($LoD = 3 \sigma/s$). The σ abbreviation is the standard deviation of the noise intensity, which was explained at the beginning of this section. The s abbreviation is the slope of the fitting line. The intensity, background and noise of the Si emissions lines were calculated, as discussed at the beginning of this section. The LoDs with and without microwaves were 3.3 ± 1 ppm and 53 ± 10 ppm using the Si 251.6 nm emission line and 1.25 ± 0.1 ppm and 18.3 ± 2.4 ppm using the Si 288.16 nm emission line. The LoD of each Si line was the average of three independent calibration curves. The uncertainty of each LoD is the standard deviation of the three LoDs.

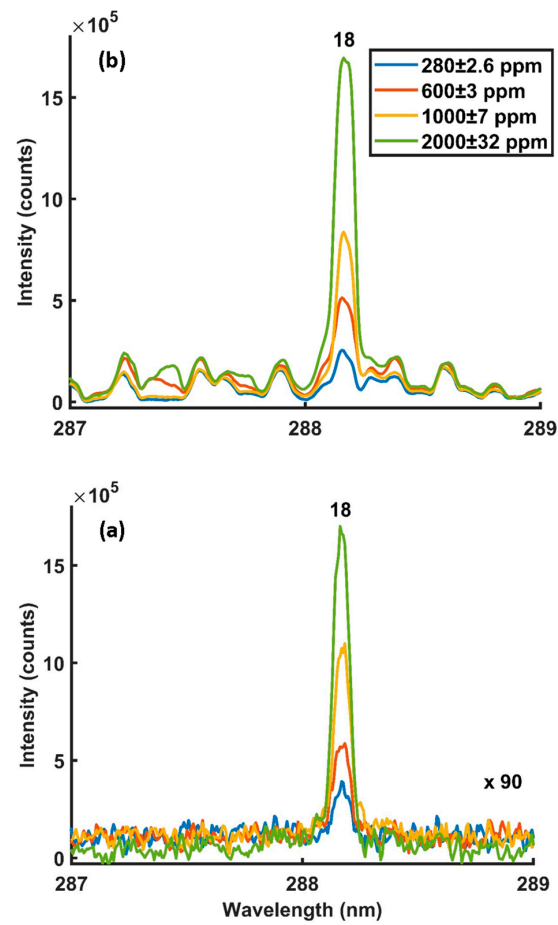


Figure 6. MA-LIBS spectra were obtained at different silicon concentrations using a Si 288.16 nm emission line: (a) microwave off and (b) microwave on. Experimental parameters: laser energy = 8 mJ; microwave power = 900 W; gate width = 900 μ s; diffraction grating = 3600 lines/mm; accumulated signals = 100; gate delay = 400 ns.

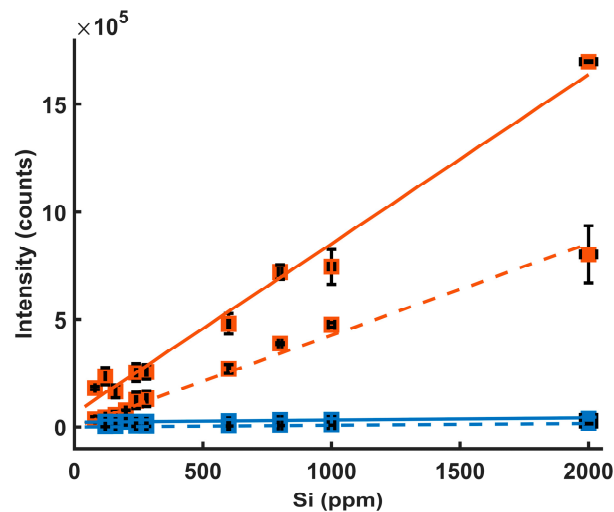


Figure 7. Calibration curves for Si in water using Si 251.6 emission line intensity (dashed lines) and 288.16 emission line intensity (solid lines) with microwave on (orange) and microwave off (blue). Experimental parameters: laser energy = 8 mJ; microwave power = 900 W; gate width = 900 μ s; diffraction grating = 3600 lines/mm; accumulated signals = 100; gate delay = 400 ns.

Although the present study performed the analysis in the liquid phase, the laser energy used and LoD were lower than their counterparts' reported values performed

in open air under ambient pressure (Table 2). For example, De Souza et al. calculated 20 ppm Si LoD using 220 mJ in open air under ambient pressure [24], and Zhang et al. used 60 mJ for ablation before using 1 mJ laser energy for SiO excitation [27]. Moreover, Skrzeczanowski et al. used 50 mJ and a sample pretreatment to achieve 5.2 ppm LoD [25]. In addition, Aragon et al. used 100 mJ laser energy to form the plasma in atmospheric Ar under ambient pressure [29]. In addition, adding a secondary laser and vacuum chamber adds more complicity to the analysis due to the multiplicity of the additional parameters that require optimisations, such as laser energy, laser pulse width, wavelength, inter-pulse gate delay, alignment and pressure [6]. However, LIBS-LIMF has one more deficiency than the rest as it gives only single-element analysis because the secondary laser wavelength is tuned to excite specific energy levels of analyte atoms [10,58]. The present study has advantages over others with a lower limit of detection in open air under ambient pressure, retaining minimal sample pretreatment and simplicity.

4. Conclusions

Microwave-assisted laser-induced breakdown spectroscopy (MA-LIBS) was demonstrated for direct silicon detection in the aqua phase for the first time. Because it uses low laser energy, MA-LIBS significantly reduces liquid splashes. An Nd:YAG laser was used to ablate the surface of the silicon solution jet to form the plasma in open air under ambient pressure, and a near-field applicator delivered microwave radiation into the plasma. The optimum parameters of laser energy and microwave power were investigated. For the analysis, 251.6 nm and 288.16 nm Si lines were nominated because they are the most intense lines of Si. The MA-LIBS recorded 51-fold and 77-fold enhancements for Si I at 251.6 nm and 288.16 nm, respectively. Four calibration curves were established for the Si analysis. The LoDs with and without microwaves were 3.3 ± 1 ppm and 53 ± 10 ppm using the Si 251.6 nm emission line and 1.25 ± 0.1 ppm and 18.3 ± 2.4 ppm using the Si 288.16 nm emission line using 8 mJ laser energy. The MA-LIBS used 8 mJ to improve the Si LoD in the liquid phase at ambient pressure and temperature conditions. Under MA-LIBS, the laser energy required for the liquid phase was lower than that needed for LIBS-LIMF and DP-LIBS applied to a solid phase. When MA-LIBS was used, the silicon LoD was 3.3 ± 1 ppm, a significant improvement over that in the previous study.

Author Contributions: Conceptualisation, Z.T.A.; methodology, A.M.A.; software, A.M.A.; validation, Z.T.A.; formal analysis, A.M.A.; investigation, A.M.A.; data curation, A.M.A.; writing—original draft preparation, A.M.A.; writing—review and editing, A.M.A.; visualisation, Z.T.A.; supervision, Z.T.A.; project administration, Z.T.A. All authors have read and agreed to the published version of the manuscript.

Funding: This research received no external funding.

Institutional Review Board Statement: Not applicable.

Informed Consent Statement: Not applicable.

Data Availability Statement: Data may be available on request.

Acknowledgments: The first author is grateful to the Jouf University for providing a PhD scholarship.

Conflicts of Interest: The authors declare no conflicts of interest.

References

1. Cremers, D.A.; Radziemski, L.J. *Handbook of Laser-Induced Breakdown Spectroscopy*, 2nd ed.; Wiley: London, UK, 2013.
2. Wilschefski, S.C.; Baxter, M.R. Inductively coupled plasma mass spectrometry: Introduction to analytical aspects. *Clin. Biochem. Rev.* **2019**, *40*, 115. [[CrossRef](#)] [[PubMed](#)]
3. Senesi, G.S.; Harmon, R.S.; Hark, R.R. Field-portable and handheld laser-induced breakdown spectroscopy: Historical review, current status and future prospects. *Spectrochim. Acta Part B At. Spectrosc.* **2021**, *175*, 106013. [[CrossRef](#)]
4. Shah, S.K.H.; Iqbal, J.; Ahmad, P.; Khandaker, M.U.; Haq, S.; Naeem, M. Laser induced breakdown spectroscopy methods and applications: A comprehensive review. *Radiat. Phys. Chem.* **2020**, *170*, 108666. [[CrossRef](#)]

5. Grebneva-Balyuk, O.; Kubrakova, I. Determination of platinum group elements in geological samples by inductively coupled plasma mass spectrometry: Possibilities and limitations. *J. Anal. Chem.* **2020**, *75*, 275–285. [[CrossRef](#)]
6. Fernandes Andrade, D.; Pereira-Filho, E.R.; Amarasiriwardena, D. Current trends in laser-induced breakdown spectroscopy: A tutorial review. *Appl. Spectrosc. Rev.* **2021**, *56*, 98–114. [[CrossRef](#)]
7. Galbács, G. A critical review of recent progress in analytical laser-induced breakdown spectroscopy. *Anal. Bioanal. Chem.* **2015**, *407*, 7537–7562. [[CrossRef](#)] [[PubMed](#)]
8. Fu, X.; Li, G.; Dong, D. Improving the detection sensitivity for laser-induced breakdown spectroscopy: A review. *Front. Phys.* **2020**, *8*, 68. [[CrossRef](#)]
9. Wang, Z.; Afgan, M.S.; Gu, W.; Song, Y.; Wang, Y.; Hou, Z.; Song, W.; Li, Z. Recent advances in laser-induced breakdown spectroscopy quantification: From fundamental understanding to data processing. *TrAC Trends Anal. Chem.* **2021**, *143*, 116385. [[CrossRef](#)]
10. Li, Y.; Tian, D.; Ding, Y.; Yang, G.; Liu, K.; Wang, C.; Han, X. A review of laser-induced breakdown spectroscopy signal enhancement. *Appl. Spectrosc. Rev.* **2018**, *53*, 1–35. [[CrossRef](#)]
11. Zheng, T.; Wang, L.; Liu, J.; Wang, J.; Jia, G. The corrosion inhibition effect of sodium silicate and Triton X-100 on 2024-T3 aluminum alloy in NaOH medium: Experimental and theoretical research. *Colloids Surf. A Physicochem. Eng. Asp.* **2021**, *610*, 125723. [[CrossRef](#)]
12. Rushing, J.C.; McNeill, L.S.; Edwards, M. Some effects of aqueous silica on the corrosion of iron. *Water Res.* **2003**, *37*, 1080–1090. [[CrossRef](#)] [[PubMed](#)]
13. Bahadori, A.; Vuthaluru, H.B. Prediction of silica carry-over and solubility in steam of boilers using simple correlation. *Appl. Therm. Eng.* **2010**, *30*, 250–253. [[CrossRef](#)]
14. Sohail, M.A.; Mustafa, A.I. Concentration control of silica in water chemical regime for natural circulation high pressure drum boiler unit of thermal power station. *Indian J. Chem. Technol.* **2007**, *14*, 195–199.
15. Nyongbela, G.N.; Johannsen, K. Laboratory-scale study on the effect of silicate on copper pipe corrosion. *Mater. Corros.* **2015**, *66*, 995–1000. [[CrossRef](#)]
16. Butcher, D.J. Recent highlights in graphite furnace atomic absorption spectrometry. *Appl. Spectrosc. Rev.* **2017**, *52*, 755–773. [[CrossRef](#)]
17. Kilmer, V.J. *Methods of Soil Analysis: Part 2 Chemical and Microbiological Properties*; Page, A.L., Ed.; American Society of Agronomy and Soil Science Society of America: Madison, WI, USA, 1983; Volume 9, pp. 263–273.
18. Montaña, M.D.; Majestic, B.J.; Jämting, Å.K.; Westerhoff, P.; Ranville, J.F. Methods for the detection and characterization of silica colloids by microsecond spICP-MS. *Anal. Chem.* **2016**, *88*, 4733–4741. [[CrossRef](#)] [[PubMed](#)]
19. Kozak, J.; Latocha, K.; Kochana, J.; Wieczorek, M.; Kościelniak, P. Simultaneous spectrophotometric flow injection determination of phosphate and silicate. *Talanta* **2015**, *133*, 150–154. [[CrossRef](#)] [[PubMed](#)]
20. Trojanowicz, M.; Pyszynska, M. Flow-Injection Methods in Water Analysis—Recent Developments. *Molecules* **2022**, *27*, 1410. [[CrossRef](#)] [[PubMed](#)]
21. Yu, X.; Li, Y.; Gu, X.; Bao, J.; Yang, H.; Sun, L. Laser-induced breakdown spectroscopy application in environmental monitoring of water quality: A review. *Environ. Monit. Assess.* **2014**, *186*, 8969–8980. [[CrossRef](#)] [[PubMed](#)]
22. Sabsabi, M.; Cielo, P. Quantitative analysis of aluminum alloys by laser-induced breakdown spectroscopy and plasma characterization. *Appl. Spectrosc.* **1995**, *49*, 499–507. [[CrossRef](#)]
23. Zheng, H.; Yueh, F.Y.; Miller, T.; Singh, J.P.; Zeigler, K.E.; Marra, J.C. Analysis of plutonium oxide surrogate residue using laser-induced breakdown spectroscopy. *Spectrochim. Acta Part B At. Spectrosc.* **2008**, *63*, 968–974. [[CrossRef](#)]
24. De Souza, P.F.; Júnior, D.S.; de Carvalho, G.G.A.; Nunes, L.C.; da Silva Gomes, M.; Guerra, M.B.B.; Krug, F.J. Determination of silicon in plant materials by laser-induced breakdown spectroscopy. *Spectrochim. Acta Part B At. Spectrosc.* **2013**, *83*, 61–65. [[CrossRef](#)]
25. Skrzeczanowski, W.; Długaszek, M. Al and Si quantitative analysis in aqueous solutions by LIBS method. *Talanta* **2021**, *225*, 121916. [[CrossRef](#)]
26. Yaroshchyk, P.; Morrison, R.J.; Body, D.; Chadwick, B.L. Quantitative determination of wear metals in engine oils using LIBS: The use of paper substrates and a comparison between single-and double-pulse LIBS. *Spectrochim. Acta Part B At. Spectrosc.* **2005**, *60*, 1482–1485. [[CrossRef](#)]
27. Zhang, W.; Zhou, R.; Liu, K.; Li, Q.; Tang, Z.; Zhu, C.; Li, X.; Zeng, X.; He, C. Silicon determination in steel with molecular emission using laser-induced breakdown spectroscopy combined with laser-induced molecular fluorescence. *J. Anal. At. Spectrom.* **2021**, *36*, 375–379. [[CrossRef](#)]
28. Abdulmajid, S.N.; Idris, N.; Pardede, M.; Jobiliong, E.; Hedwig, R.; Lie, Z.S.; Suyanto, H.; Tjia, M.O.; Kurniawan, K.H.; Kagawa, K. Sensitive analysis of carbon, chromium and silicon in steel using picosecond laser induced low pressure helium plasma. *Spectrochim. Acta Part B At. Spectrosc.* **2015**, *114*, 1–6. [[CrossRef](#)]
29. Aragon, C.; Aguilera, J.A.; Penalba, F. Improvements in quantitative analysis of steel composition by laser-induced breakdown spectroscopy at atmospheric pressure using an infrared Nd: YAG laser. *Appl. Spectrosc.* **1999**, *53*, 1259–1267. [[CrossRef](#)]
30. Ismail, M.A.; Cristoforetti, G.; Legnaioli, S.; Pardini, L.; Palleschi, V.; Salvetti, A.; Tognoni, E.; Harith, M.A. Comparison of detection limits, for two metallic matrices, of laser-induced breakdown spectroscopy in the single and double-pulse configurations. *Anal. Bioanal. Chem.* **2006**, *385*, 316–325. [[CrossRef](#)]

31. Kasim, A.F.A.; Wakil, M.; Grant, K.; Hearn, M.; Alwahabi, Z.T. Aqueous ruthenium detection by microwave-assisted laser-induced breakdown spectroscopy. *Plasma Sci. Technol.* **2022**, *24*, 084004. [CrossRef]
32. Ikeda, Y.; Soriano, J.K.; Wakaida, I. Signal-to-noise ratio improvements in microwave-assisted laser-induced breakdown spectroscopy. *Talanta Open* **2022**, *6*, 100138. [CrossRef]
33. Viljanen, J.; Sun, Z.; Alwahabi, Z.T. Microwave assisted laser-induced breakdown spectroscopy at ambient conditions. *Spectrochim. Acta Part B At. Spectrosc.* **2016**, *118*, 29–36. [CrossRef]
34. Wall, M.; Sun, Z.; Alwahabi, Z.T. Quantitative detection of metallic traces in water-based liquids by microwave-assisted laser-induced breakdown spectroscopy. *Opt. Express* **2016**, *24*, 1507–1517. [CrossRef] [PubMed]
35. Wakil, M.; Alwahabi, Z.T. Microwave-assisted laser induced breakdown molecular spectroscopy: Quantitative chlorine detection. *J. Anal. At. Spectrom.* **2019**, *34*, 1892–1899. [CrossRef]
36. Wakil, M.; Alwahabi, Z.T. Quantitative fluorine and bromine detection under ambient conditions via molecular emission. *J. Anal. At. Spectrom.* **2020**, *35*, 2620–2626. [CrossRef]
37. Ikeda, Y.; Soriano, J.K. Microwave-enhanced laser-induced air plasma at atmospheric pressure. *Opt. Express* **2022**, *30*, 33756–33766. [CrossRef]
38. Ikeda, Y. Atmospheric air plasma sustainment by semiconductor microwave for hydroxyl radical production and powder metal element analysis. *Opt. Express* **2022**, *30*, 29868–29884. [CrossRef] [PubMed]
39. Cai, S.; Tang, Y.; Wang, F.; Xiong, Y.; Sun, X.; Ming, X. Investigation of the multi-elemental self-absorption mechanism and experimental optimization in laser-induced breakdown spectroscopy. *J. Anal. At. Spectrom.* **2020**, *35*, 912–926. [CrossRef]
40. Tang, Y.; Li, J.; Hao, Z.; Tang, S.; Zhu, Z.; Guo, L.; Li, X.; Zeng, X.; Duan, J.; Lu, Y. Multielemental self-absorption reduction in laser-induced breakdown spectroscopy by using microwave-assisted excitation. *Opt. Express* **2018**, *26*, 12121–12130. [CrossRef] [PubMed]
41. Fortes, F.J.; Moros, J.; Lucena, P.; Cabalín, L.M.; Laserna, J.J. Laser-induced breakdown spectroscopy. *Anal. Chem.* **2013**, *85*, 640–669. [CrossRef] [PubMed]
42. Keerthi, K.; George, S.D.; Kulkarni, S.D.; Chidangil, S.; Unnikrishnan, V. Elemental analysis of liquid samples by laser induced breakdown spectroscopy (LIBS): Challenges and potential experimental strategies. *Opt. Laser Technol.* **2022**, *147*, 107622. [CrossRef]
43. Neumann, W. *Fundamentals of Dispersive Optical Spectroscopy Systems*; SPIE Press: Bellingham, WA, USA, 2014.
44. Ball, D.W. *The Basics of Spectroscopy*; SPIE Press: Bellingham, WA, USA, 2001; Volume 49.
45. Chen, S.J.; Iqbal, A.; Wall, M.; Fumeaux, C.; Alwahabi, Z.T. Design and application of near-field applicators for efficient microwave-assisted laser-induced breakdown spectroscopy. *J. Anal. At. Spectrom.* **2017**, *32*, 1508–1518. [CrossRef]
46. Al Shuaili, A.A.; Al Hadhrami, A.M.; Wakil, M.; Alwahabi, Z.T. Improvement of palladium limit of detection by microwave-assisted laser induced breakdown spectroscopy. *Spectrochim. Acta Part B At. Spectrosc.* **2019**, *159*, 105666. [CrossRef]
47. Kramida, A.; Ralchenko, Y.; Reader, J.; Team, N.A. NIST Atomic Spectra Database (ver. 5.11). 2023. Available online: <https://www.nist.gov/pml/atomic-spectra-database> (accessed on 1 November 2023).
48. Pearse, R.W.B.; Gaydon, A.G.; Pearse, R.W.B.; Gaydon, A.G. *The Identification of Molecular Spectra*; Chapman and Hall: London, UK, 1976; Volume 297.
49. Lasheras, R.; Bello-Gálvez, C.; Anzano, J. Quantitative analysis of oxide materials by laser-induced breakdown spectroscopy with argon as an internal standard. *Spectrochim. Acta Part B At. Spectrosc.* **2013**, *82*, 65–70. [CrossRef]
50. Yi, R.; Li, J.; Yang, X.; Zhou, R.; Yu, H.; Hao, Z.; Guo, L.; Li, X.; Zeng, X.; Lu, Y. Spectral interference elimination in soil analysis using laser-induced breakdown spectroscopy assisted by laser-induced fluorescence. *Anal. Chem.* **2017**, *89*, 2334–2337. [CrossRef] [PubMed]
51. Jolivet, L.; Leprince, M.; Moncayo, S.; Sorbier, L.; Lienemann, C.-P.; Motto-Ros, V. Review of the recent advances and applications of LIBS-based imaging. *Spectrochim. Acta Part B At. Spectrosc.* **2019**, *151*, 41–53. [CrossRef]
52. Tognoni, E.; Palleschi, V.; Corsi, M.; Cristoforetti, G. Quantitative micro-analysis by laser-induced breakdown spectroscopy: A review of the experimental approaches. *Spectrochim. Acta Part B At. Spectrosc.* **2002**, *57*, 1115–1130. [CrossRef]
53. Palleschi, V. Avoiding Misunderstanding self-Absorption in laser-induced breakdown spectroscopy (LIBS) analysis. *Spectroscopy* **2022**, *37*, 60–62. [CrossRef]
54. Alamri, A.M.; Viljanen, J.; Kwong, P.; Alwahabi, Z.T. Isotope Detection in Microwave-Assisted Laser-Induced Plasma. *Plasma* **2023**, *6*, 466–477. [CrossRef]
55. Liu, Y.; Baudelet, M.; Richardson, M. Elemental analysis by microwave-assisted laser-induced breakdown spectroscopy: Evaluation on ceramics. *J. Anal. At. Spectrom.* **2010**, *25*, 1316–1323. [CrossRef]
56. Iqbal, A.; Sun, Z.; Wall, M.; Alwahabi, Z.T. Sensitive elemental detection using microwave-assisted laser-induced breakdown imaging. *Spectrochim. Acta Part B At. Spectrosc.* **2017**, *136*, 16–22. [CrossRef]
57. Ikeda, Y.; Soriano, J.K.; Kawahara, N.; Wakaida, I. Spatially and temporally resolved plasma formation on alumina target in microwave-enhanced laser-induced breakdown spectroscopy. *Spectrochim. Acta Part B At. Spectrosc.* **2022**, *197*, 106533. [CrossRef]
58. Goueguel, C.; Laville, S.; Vidal, F.; Chaker, M.; Sabsabi, M. Resonant laser-induced breakdown spectroscopy for analysis of lead traces in copper alloys. *J. Anal. At. Spectrom.* **2011**, *26*, 2452–2460. [CrossRef]

Disclaimer/Publisher’s Note: The statements, opinions and data contained in all publications are solely those of the individual author(s) and contributor(s) and not of MDPI and/or the editor(s). MDPI and/or the editor(s) disclaim responsibility for any injury to people or property resulting from any ideas, methods, instructions or products referred to in the content.